Journal of Solid State Chemistry 210 (2014) 150–154

Contents lists available at ScienceDirect

Journal of Solid State Chemistry

journal homepage: www.elsevier.com/locate/jssc

The pressure-induced phase transition studies of In_2S_3 and In_2S_3:Ce nanoparticles

Binbin Yao, Hongyang Zhu, Shuangming Wang, Pan Wang, Mingzhe Zhang*

State Key Laboratory of Superhard Materials, Jilin University, Changchun 130012, People's Republic of China

ARTICLE INFO

Article history:
Received 30 July 2013
Received in revised form
31 October 2013
Accepted 3 November 2013
Available online 20 November 2013

Keywords:
High-pressure phase transition
Doped ions
Defect structure
Lattice distortion
Structural stability

ABSTRACT

A novel method, gas–liquid phase chemical deposition is developed to prepare In_2S_3 and In_2S_3:Ce nanoparticles. The structural, morphology and composition feature of these two nanoparticles is studied by XRD, HRTEM, and XPS. *In situ* high-pressure synchrotron X-ray diffraction studies were carried out by using a diamond-anvil cell. The doping does not influence the tetragonal-to-cubic phase transition path while results in a lower phase transition pressure of In_2S_3:Ce nanoparticles (4.3 GPa) than that of In_2S_3 nanoparticles (7.1 GPa). The bulk moduli of tetragonal phases are $B_0=87.1\pm4.3$ GPa and $B_0=55.6\pm4.1$ GPa, respectively. The distinct high-pressure behaviors can be explained in term of the doped ions, causing lattice distortion and reducing structural stability of the In_2S_3 nanoparticles and further accelerating the phase transition.

1. Introduction

Metal chalcogenides have extremely attracted attention due to the unique physical and chemical properties [1–3]. Transition or rare-earth metal atoms are introduced into the cationic sites of a semiconducting host lattice, which are close to materials used in microelectronics and exhibit simultaneously semiconducting and ferromagnetic properties [4–6]. In_2S_3 has been widely noticed owing to its special spinel structure with a large amount of vacancies, which cause a number of quasi-interstitial cations and an equal number of cation vacancies [7–9]. A considerable degree of disorder results in the application of red and green phosphors, and is useful for doping transition or rare-earth metals in the kind of materials. Doped In_2S_3 presents a larger number of defects and the changes of electronic density distribution and band gap, these structural parameters will ultimately determine the functional properties of the nanomaterials [10–14]. Moreover, doping is an effective way to adjust the microstructure of nanocrystals. And some researches show that the change of microstructure further will have effect on its high-pressure behavior. Therefore, the high-pressure study of doped In_2S_3 can explore the change of micro-structure. And the studies show high pressure is a feasible approach to tune and synthesize phase structure. However, there is no report about the high-pressure study of In_2S_3.

High-pressure researches on nanostructural materials have been of a considerably interest because of the appearance of many novel high-pressure behaviors in the nanomaterials [15–17]. As we all know, the high pressure tunes the distance and interaction between atoms or molecules, and discovers new pressure-induced phases and phenomenon, the results under high pressure condition are different from that under the atmospheric pressure [18–20]. Previous high-pressure studies of nanocrystalline show that the size, shape, and structure of the materials (vacancies, dislocations, stacking faults, etc) have significant effects on the phase transition pressure, compressibility, and even phase transition routines [21–23], in which the size effect of nanomaterials is the most important factor. In addition, the phase transition is a function of the structural stability. For instance, the subtle incorporation of soft ligands in CdSe nanosheets and a series of defect activities being silent in ZnS can enhance the structural stability causing delay of the phase transition[24,25]; and the doping in the compound reduces the structural stability, leading to the decrease of phase transition pressure [26–29]. These results indicate that the defect ratio is responsible for the structural stability, and the doping has an effect on the phase transition pressure due to the presence of defects. It is well known that the radius and electronegativity of dopant are different from those of the cations in the host material, and a nonhomogeneous distribution of dopant favors the formation of doped ions enriched areas and some isolated doped ions, so doping atoms can cause lattice distortion and reduce the structural stability, leading to a significant influence on the phase transition [30].

In this work, the In_2S_3 and In_2S_3:Ce nanoparticles are synthesized by gas–liquid phase chemical deposition. The nanoparticles

* Corresponding author.
E-mail address: zhangmz@jlu.edu.cn (M. Zhang).

0022-4596/$ - see front matter © 2013 Elsevier Inc. All rights reserved.
http://dx.doi.org/10.1016/j.jssc.2013.11.009

size of the pure and doped In_2S_3 both are 5–6 nm. There are direct comparative high-pressure studies between In_2S_3 and In_2S_3:Ce, the comparative subtle approach excludes the size effect of nanomaterials and allows effective detection of the indeed different high-pressure behaviors between In_2S_3 and In_2S_3:Ce nanoparticles. The phase transition of the In_2S_3 and In_2S_3:Ce nanoparticles have been investigated for the first time by *in situ* high pressure synchrotron X-ray in a diamond anvil cell. The contrast of the phase transition path, the transition pressure and bulk moduli embody the different pressure-induced behavior. The unusual high-pressure behaviors observed in In_2S_3:Ce nanoparticles have been discussed in term of the effects of volume expansion, volume collapse and structural defects on phase transition.

2. Experiment details

The In_2S_3 and In_2S_3:Ce nanoparticles used in this experiment were synthesized by an easily reproducible gas–liquid phase chemical deposition by using $In(COOCH_3)_3 \cdot 3H_2O$, Ce $(COOCH_3)_3 \cdot 6H_2O$ and H_2S as source materials. The experimental set-up and steps are shown in Fig. 1. The H_2S gas was prepared by HCl reacting with Na_2S. In the reaction process, H_2S gas and the reactive solution reacted in a chamber with circulating water (25 °C), which keeps the stability of reaction conditions. The chamber was set in the ultrasonic to avoid the nanoparticles forming aggregates and propel the new liquid surface emerging, which then reacted with the flowing H_2S gas. In the beginning, numerous nuclei were formed and started to grow on gas–liquid interface. Under the effect of ultrasound, the particle invaded into the solution, the new liquid surface emerged. This process was repeated until the reaction was fully completed. The precipitates were collected and washed with deionized water and anhydrous alcohol three times respectively by centrifugation, and dried in a nitrogen atmosphere.

The phase purity and structure of the nanocrystals were observed with an X-ray diffraction (XRD) (Shimadzu, XRD-6000), further analyzed morphology and size with HRTEM (TECNAI G2), and obtain the detail composition with XPS (ESCALAB MK II). Subsequently, the high-pressure XRD experiments performed on the as-prepared samples at Cornell High Energy Synchrotron Source (λ=0.485946 Å). High pressure was generated in a diamond anvil cell with a culet size of 400 μm in diameter. Silicone oil was used as the pressure transmitting medium [30,31]. The samples and medium were loaded into a hole of 150 μm in diameter drilled in the center of a pre-indented T301 stainless steel gasket. The pressure was calibrated by the frequency shift of the ruby R_1 fluorescence line. The XRD data were collected by using a MAR345 imaging plate. The two dimensional (2D) data were transferred to one dimensional (1D) powder diffraction patterns by using the software package Fit2D.

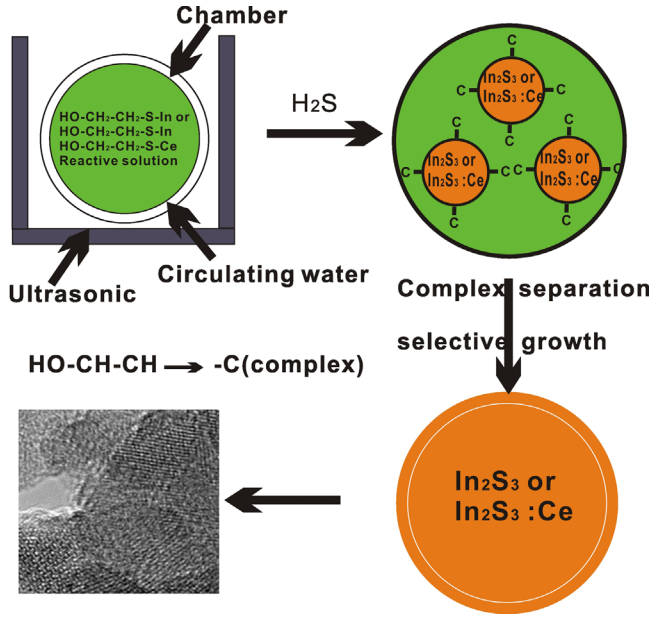

Fig. 1. The scheme of the experimental set-up and steps, the chamber with circulating water setting in the ultrasonic, the H_2S gas flow be controlled by gas flowmeter.

3. Results and discussion

The typical X-ray diffraction patterns with Cu $K\alpha 1$ (λ=1.5406 Å) of the In_2S_3 and In_2S_3:Ce nanocrystals are shown in Fig. 2. It can be seen that all of the diffraction peaks can be indexed to the standard In_2S_3 (JCPDS No 25-390, space group: I41/amd (No. 141)). The diffraction peaks of impurities are not observed. However, it can be observed that the peak position of the In_2S_3:Ce nanoparticles shift slightly toward lower angle (higher d value) comparing with the In_2S_3 nanocrystals. It is suggested that the doping causes lattice distortion due to the bigger radius of Ce atoms (r_{Ce}1.034 > r_{In}0.8), and then increase the corresponding lattice parameters. The lattice parameters of In_2S_3 nanoparticals at ambient calculated by the UNITCELL software are a=7.62368 (6) Å and c=32.35897 (7) Å, corresponding unit cell volume (V_0) is 1880.72 (1) Å^3; and the calculated lattice parameters of In_2S_3:Ce nanoparticles are a=7.68028 (6) Å, c=32.51783 (2) Å and V_0=1918.11 (1) Å^3, which are obviously larger than the In_2S_3 nanoparticles, indicating that the doped ions lead to the volume expansion (lattice distortion).

The morphology features of the as-prepared samples, typical high resolution transmission electron microscopy (HRTEM) images are shown in Fig. 3. The results reveal that the diffraction rings correspond to the X-ray diffraction patterns without any impurities, and the morphology is particle in Fig. 3(a) and (c). Fig. 3(b) and (d) are the High Resolution Transmission Electron Microscopy of two samples. The particles sizes are 5–6 nm with the interplanar spacing being 0.32 nm and 0.27 nm and the clearly lattice fringes are shown in Fig. 3(b) and (d).

The X-ray photoelectron spectroscopy (XPS) are investigated to further obtain the detailed composition of the In_2S_3 and In_2S_3:Ce nanoparticles with doping Ce content 3%. The In and S peaks can be found in the pure and doped In_2S_3 nanoparticles, as shown in Fig. 4(a–d). The Ce peaks of the In_2S_3:Ce nanoparticles have been detected as shown in Fig. 4(e). The binding energies for Ce $3d_{5/2}$

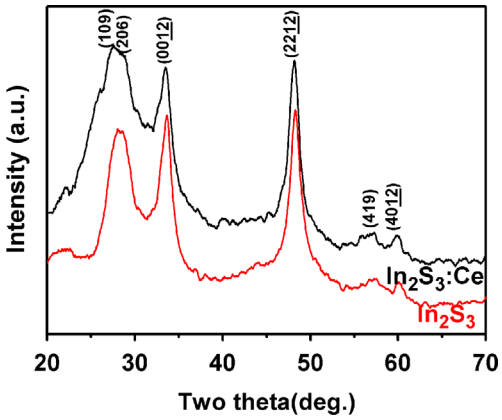

Fig. 2. X-ray diffraction (XRD) about In_2S_3 and In_2S_3:Ce nanoparticles, and the peak position of In_2S_3:Ce nanoparticles shift to the low angle comparing with that of the In_2S_3 nanoparticles.